Configurations of the low-lying states in ^{146}Eu

Q. B. Zeng,[1,2] S. Guo,[1,2,*] Z. Liu,[1,2,†] J. G. Li,[1,2] H. H. Li,[1,2] J. G. Wang,[1] Z. Y. Zhang,[1] L. Ma,[1] Y. H. Qiang,[1] M. H. Huang,[1,2] G. S. Li,[1,2] Y. D. Fang,[1,2] M. L. Liu,[1,2] B. Ding,[1] Y. Zheng,[1,2] J. H. Li,[1,2] H. Y. Lu,[1,2] W. Q. Zhang,[1,2] K. L. Wang,[1] X.Y Liu,[1,2] H. Huang,[1,2] F. F. Zeng,[1,2] X. H. Yu,[1,2] A. Rohilla,[3] J. F. Huang,[4] H. L. Fan,[5] C. Qi,[6] C. X. Yuan,[7] C. M. Petrache,[8] E. A. Lawrie,[9,10] W. Zuo,[1,2] Z. G. Gan,[1,2] and X. H. Zhou[1,2]

[1] *Institute of Modern Physics, Chinese Academy of Sciences, Lanzhou 730000, People's Republic of China*
[2] *School of Nuclear Science and Technology, University of Chinese Academy of Science, Beijing 100049, People's Republic of China*
[3] *Shandong Provincial Key Laboratory of Optical Astronomy and Solar-Terrestrial Environment, Institute of Space Sciences, Shandong University, Weihai 264209, People's Republic of China*
[4] *Guangzhou Municipal Ecological Environment Bureau Huadu District Branch, Guangzhou 510800, People's Republic of China*
[5] *College of Engineering Physics, Shenzhen Technology University, Shenzhen 518118, People's Republic of China*
[6] *Department of Physics, Royal Institute of Technology, Stockholm 104 05, Sweden*
[7] *Sino-French Institute of Nuclear Engineering and Technology, Sun Yat-Sen University, Zhuhai 519082, Guangdong, People's Republic of China*
[8] *University Paris-Saclay, CNRS/IN2P3, IJCLab, 91405 Orsay, France*
[9] *iThemba LABS, National Research Foundation, P.O. Box 722, Somerset West 7131, South Africa*
[10] *Department of Physics & Astronomy, University of the Western Cape, P/B X17, Bellville 7535, South Africa*

(Received 10 January 2022; revised 4 June 2022; accepted 18 August 2022; published 14 September 2022)

The low-lying states of ^{146}Eu populated in the decay of the 9^+ isomer were studied. The γ-ray intensities were reanalyzed employing germanium detectors, and the lifetimes of the 6^-_1 and 6^-_2 states were measured using the mirror symmetric centroid difference (MSCD) method with fast-timing $LaBr_3(Ce)$ scintillator detectors. The $B(M1)$ values of the $6^-_1 \rightarrow 5^-_1$ and $6^-_2 \rightarrow 5^-_1$ transitions were deduced, and all observed states were interpreted as members of the $\pi d^{-1}_{5/2} \nu f_{7/2}$ and $\pi g^{-1}_{7/2} \nu f_{7/2}$ multiplets. In particular, the 5^-_1 level is shown to be dominated by the $\pi d^{-1}_{5/2} \nu f_{7/2}$ configuration, solving the discrepancy in its configuration assignment proposed in previous works. These experimental results were compared with the shell model calculations using several different effective interactions. The systematics of low-lying structure in the $N = 83$ isotones ^{142}Pr, ^{144}Pm, and ^{146}Eu was established.

DOI: 10.1103/PhysRevC.106.034307

I. INTRODUCTION

Nuclei with few valence nucleons with respect to a core are among the best candidates to constrain the single-particle potential and the effective residual interaction employed in shell model calculations [1–4]. Experimentally, a lot of multiplets in odd-odd nuclei around doubly closed shell nuclei have been identified [5–10], and their excitation energies were used to extract the neutron-proton (*n-p*) interaction [2,5,11]. Several investigations pointed out that the ^{146}Gd nucleus can be considered as a doubly closed shell nucleus, despite the shell closures not being as pronounced as in ^{208}Pb [12–15]. Thus, the odd-odd nuclei around ^{146}Gd are expected to offer opportunities to study the *n-p* interaction in this mass region. On the other hand, it is often difficult to match the experimentally observed levels with the calculated ones due to the uncertainty in the shell model calculations, especially for the odd-odd nuclei which have higher level densities. To pin down the level configurations, detailed experimental information, in particular reduced transition probabilities, is needed.

Lifetime is an essential observable for extracting the reduced transition probability, and directly reflects the overlap between the wave functions of the initial and final states [16,17]. Although many experiments have been performed to study the low-lying levels in the $A \approx 140$ region, data on lifetimes and transition moments are still rare. Among these studies, the fast timing method is commonly applied in β-decay experiments, but states populated by β decay are limited due to the selection rules. The Doppler-shift attenuation method (DSAM) [18] and recoil distance Doppler-shift (RDDS) method [19] are able to measure lifetimes in the picosecond range, and are mainly applied in in-beam experiments, but are hampered by the presence of μs isomers originated from the $\pi h_{11/2}$ orbital in this mass region [20].

The low-lying states in ^{146}Eu, resulting from the coupling of one neutron particle to one proton hole with respect to the ^{146}Gd core, provide the opportunity to study the *n-p* interaction in this mass region. These states have been investigated in several experiments [21–25], where the J^π of the levels below the 9^+ isomer were determined. So far, only the lifetimes

*Corresponding author: gs@impcas.ac.cn
†Corresponding author: liuzhong@impcas.ac.cnn

of the 2^- and 3^- levels have been reported [21]. For the 5_1^- state, a $\pi d_{5/2}^{-1}\nu f_{7/2}$ configuration was proposed by Ercan *et al.* [22,24], while a $\pi g_{7/2}^{-1}\nu f_{7/2}$ configuration was suggested based on a shell model calculation by Bhattacharjee *et al.* [21]. In Refs. [22,24], the first and second 6^- levels were assigned to the $\pi d_{5/2}^{-1}\nu f_{7/2}$ and $\pi g_{7/2}^{-1}\nu f_{7/2}$ multiplets, respectively. But the reduced transition probabilities between the 9^+ isomer and these two 6^- levels were found to differ by a factor of 5 [22,24], a discrepancy with the similar reduced transition probabilities from the 7^- state to the two 6^- states [22,26].

In the present work, the fusion-evaporation residues of the ^{124}Sn(^{27}Al, $5n$) reaction were delivered to the focal plane of a gas-filled recoil separator and the nuclear states of interest were populated by isomeric decay. The γ-ray intensities were reextracted employing germanium detectors, and the lifetimes of the 6_1^- and 6_2^- states were measured using the MSCD method with fast-timing $LaBr_3$ detectors. The $B(M1)$ values of the $6_1^- \rightarrow 5_1^-$ and $6_2^- \rightarrow 5_1^-$ transitions were deduced. All observed states can be experimentally interpreted as members of the $\pi d_{5/2}^{-1}\nu f_{7/2}$ and $\pi g_{7/2}^{-1}\nu f_{7/2}$ multiplets, and this conclusion was compared with the shell model calculations. In particular, the main configuration of the first 5^- state is determined as $\pi d_{5/2}^{-1}\nu f_{7/2}$, different from that proposed in Ref. [21].

II. EXPERIMENTAL DETAILS

The ^{146}Eu isotope was produced in the ^{124}Sn(^{27}Al, $5n$) reaction with an isotopically enriched (96.96%) ^{124}Sn target. The ^{27}Al beam was accelerated to 127 MeV by the Sector-Focusing Cyclotron (SFC) of the Heavy Ion Research Facility in Lanzhou (HIRFL). The target consisted of Au foils with a thickness of 2.3 mg/cm^2 facing the beam, a 300-μg/cm^2-thick ^{124}Sn metal layer, and a $^{124}SnO_2$ layer of thickness 160 μg/cm^2.

Evaporation residues (ERs) were separated by the gas-filled recoil separator, Spectrometer for Heavy Atoms and Nuclear Structure (SHANS) [27], and implanted in a 50 × 50 mm^2 size and 300-μm-thick single silicon detector (SSD). The time of flight (TOF) of the ERs in SHANS is about 1 μs. To minimize the interference from scattered light ions in the implantation SSD, one Si detector of 50 × 50 mm^2 size was placed behind the implantation SSD detector to serve as a veto detector. The implantation and veto detectors were both placed inside an aluminum collection chamber. Around the chamber, five γ-ray detectors were installed, including three fast-timing $LaBr_3$(Ce) scintillator detectors, one coaxial high-purity germanium detector (HPGe), and one segmented clover-type HPGe detector. A schematic view of the detection system is presented in Fig. 1. The energy, time, as well as relative efficiency calibrations were carried out using a ^{152}Eu γ source. The typical energy resolutions (FWHM) of Ge and $LaBr_3$ detectors for the 344-keV γ ray of ^{152}Eu are about 3 and 31 keV, respectively. The typical γ-γ timing resolution of the $LaBr_3$(Ce) detectors is 330 ps for coincidence between the 344- and 779-keV transitions of ^{152}Eu. The lifetimes of the levels were obtained using the γ-γ fast-timing technique employing the $LaBr_3$(Ce) detectors. The HPGe and clover detectors were used to identify the characteristic γ rays and extract the γ-ray intensities.

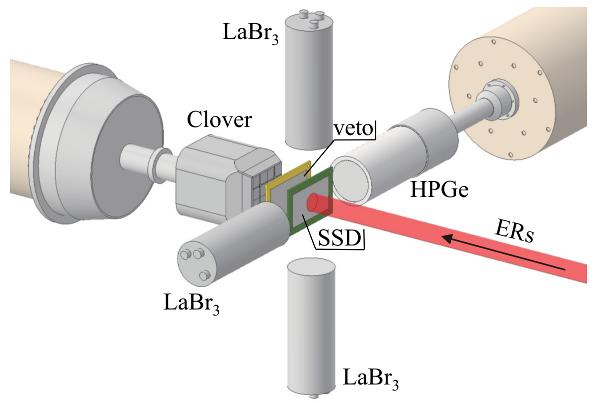

FIG. 1. A schematic view of the detection system, which consists of one single silicon detector, one veto, three $LaBr_3$(Ce) scintillator detectors, and two Ge detectors.

Typical implantation rate in the SSD detector was about 2000 particles/s. For the isomeric decay with a lifetime shorter than 500 μs, the γ background can be reduced by choosing an appropriate time window between the γ rays and implantations.

The lifetimes of the excited levels of interest were measured employing the mirror symmetric centroid difference (MSCD) method with $LaBr_3$(Ce) detectors as proposed by Régis *et al.* [28–30]. The obtained time centroid difference $\Delta C_{\mathrm{gross}}$ is a linear combination of time centroid difference of full-energy peaks and that of the corresponding background:

$$\Delta C_{\mathrm{gross}} = \frac{\Pi \Delta C + \Delta C_{\mathrm{B}}}{1 + \Pi}, \tag{1}$$

where Π is the peak-to-background ratio, ΔC_{B} is the time centroid difference of the background underneath the full-energy peaks, and ΔC is the true centroid difference. Then the background-corrected lifetime is

$$\tau = \frac{1}{2}\left[\Delta C_{\mathrm{gross}} + \frac{\Delta C_{\mathrm{gross}} - \Delta C_{\mathrm{B}}}{\Pi} - \Delta \mathrm{C(P)}\right]. \tag{2}$$

For any energy combination $\Delta E_\gamma = E_{\mathrm{feeder}} - E_{\mathrm{decay}}$, the prompt centroid difference $\Delta C(\mathrm{P})$ can be obtained from the energy dependent PRD curve, generated from the $\Delta C(\mathrm{P})$ plot against E_γ using a prompt γ source. It is worth noting that ΔC_{B} was obtained by linear interpolation of the background time centroid differences.

III. EXPERIMENTAL RESULTS

To validate the present experimental setup, we extracted the lifetime of the 2^+ state in ^{146}Sm using the MSCD method. The γ-ray intensities in ^{146}Eu were re-extracted, and the lifetimes of the first and second 6^- states were measured.

A. The prompt response difference (PRD) curve

The PRD curve obtained by using the ^{152}Eu source is shown in Fig. 2(a). Data points correspond to transitions

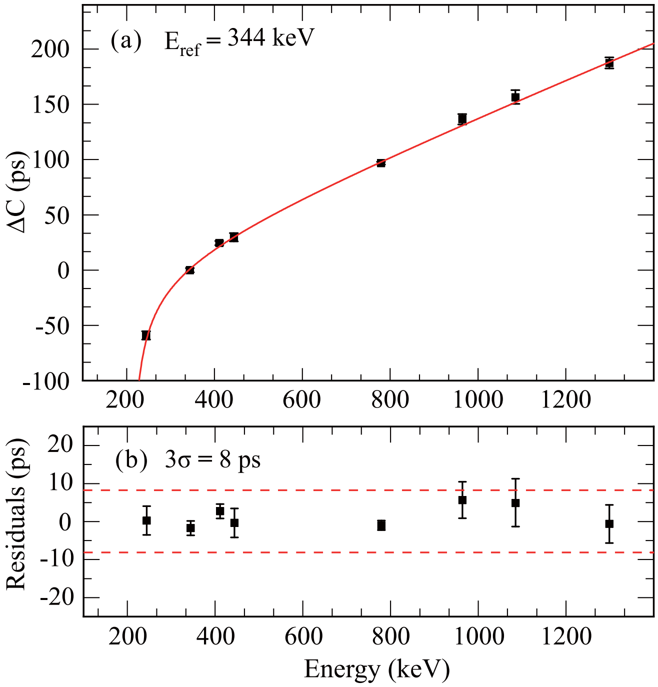

FIG. 2. (a) The PRD curve of the γ-γ fast timing setup obtained using the ^{152}Eu source. (b) Fitted residuals of the PRD curve. The dashed lines indicate a 3σ deviation corresponding to 8 ps, which represents the uncertainty of time calibration.

depopulating prompt states in ^{152}Sm and ^{152}Gd. The function fitted to the data has the form [29]

$$\mathrm{PRD}(E_\gamma) = \frac{a}{\sqrt{(b+E_\gamma)}} + cE_\gamma + d, \tag{3}$$

where a, b, c, and d are the fit parameters. Figure 2(b) shows the uncertainty of the PRD, represented by the dashed lines corresponding to three standard deviations (σ).

B. Validation of the present setup with ^{146}Sm

The excited states of ^{146}Sm were populated in the β decay of ^{146}Eu. The lifetime of the first 2^+ state in ^{146}Sm was determined using the MSCD method. Figure 3 shows the HPGe and LaBr$_3$(Ce) spectra gated by the 747-keV γ ray, which shows that the 633- and 634-keV transitions were well populated, while the 665-, 701-, and 702-keV γ rays of ^{146}Sm were also recorded. The delayed (decay transition taken as stop signal) and antidelayed (feeding transition detected as stop signal) time spectra are shown in Fig. 4, and the corresponding time centroid difference is $\Delta C_{\mathrm{gross}} = -21(4)$ ps. The background correction procedure is applied using Eq. (2), in which the ΔC_{B} was estimated by linear interpolation of the background time centroid differences from the coincidences between the 747-keV γ ray and two background gates (shown in Fig. 3), and found to be $\Delta C_{\mathrm{B}} = -39(13)$ ps. The resulting true centroid difference is derived as $\Delta C_{2_1^+} = -18(5)$ ps. Then the background-corrected lifetime of the 2_1^+ state was deduced as $\tau_{2_1^+} = 2^{+5}_{-2}$ ps, in agreement with the previous value of $7.3^{+3.0}_{-7.3}$ ps reported by Rozak *et al.* using the recoil distance method (RDM) [32].

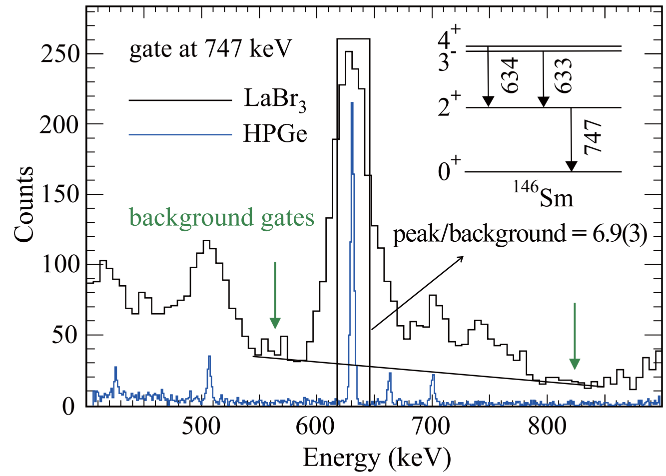

FIG. 3. Coincident γ-ray spectra gated by 747 keV. The histogram in black is the LaBr$_3$ spectrum, and the blue one is the Ge spectrum. The inset shows the partial level scheme of ^{146}Sm [31] relevant to the present measurement.

C. γ-ray intensity extraction

The excited states in ^{146}Eu studied here were populated by isomer decay. Figure 5 shows the excited states below the 9^+ isomer [24] observed in the present experiment, and Fig. 6 presents the relevant γ spectra. The coincident spectra were measured between 10 and 700 μs after the residuals were implanted in the SSD. From the γ signals recorded by the HPGe detectors and implantation signals recorded by the SSD, the half-life of the 9^+ isomer was extracted to be 230(6) μs, in agreement with the evaluated value of 235(3) μs [33]. The γ-ray intensities of the 294- and 316-keV transitions, together with the summed intensities of the 275- and 358-keV doublets, were deduced and normalized to intensity of the 377-keV γ ray, consistent with the literature value [22]. In the

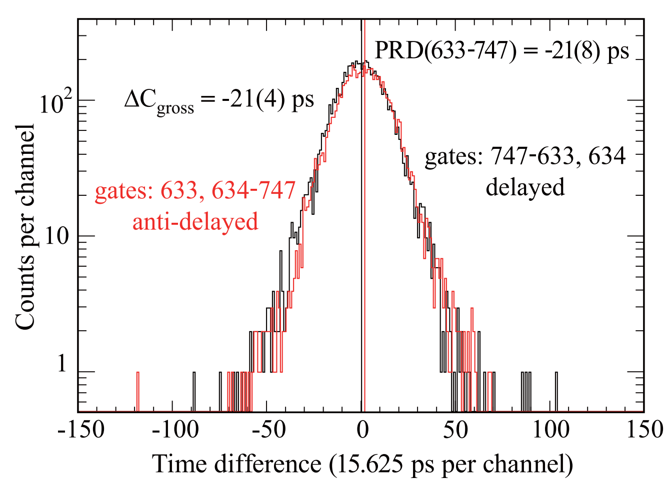

FIG. 4. Delayed and antidelayed time-difference spectra for the first 2^+ state in ^{146}Sm.

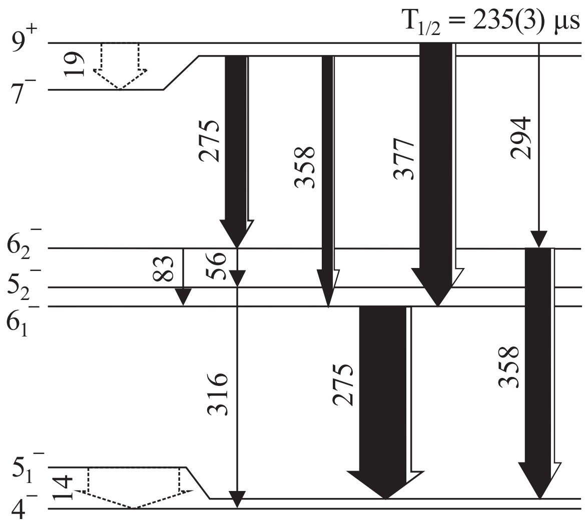

FIG. 5. The relevant level scheme below the 9^+ isomer of ^{146}Eu [24]. The widths of the arrows are proportional to the intensities extracted in the present work (see Table I). The half-life of the 9^+ isomer comes from Ref. [33]. Dashed lines indicate the transitions that were adopted in Ref. [24] but not observed in the present experiment.

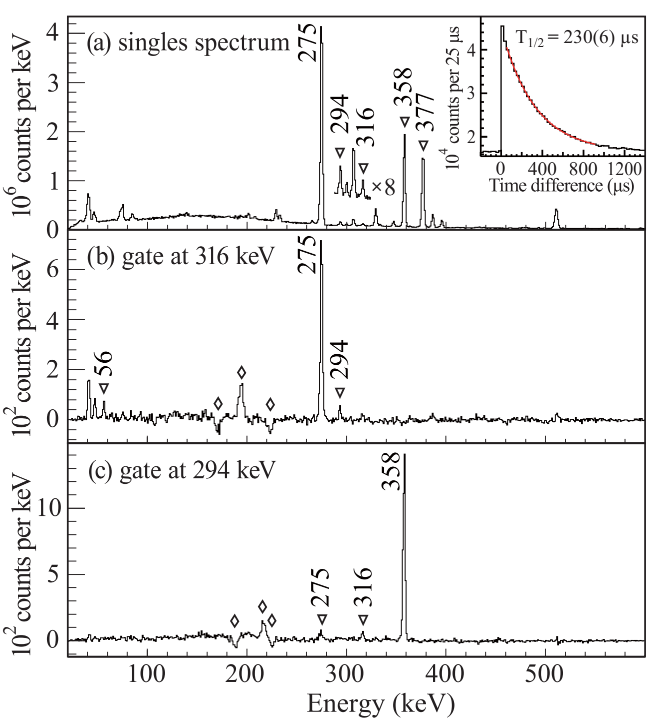

FIG. 6. Panel (a) presents the singles spectrum detected by clover and coaxial HPGe detectors. Panels (b) and panel (c) show the coincident γ-ray spectra gated on the 316- and 294-keV peaks, respectively. The coincident spectra were collected between 10 and 700 μs after the residuals were implanted in the SSD. Time distribution of the 377-keV γ ray is shown in the inset. The peaks from the scattering of 511-keV γ ray in panels (b) and (c) were marked with diamond symbols.

316-keV gated spectrum, the 275-keV peak only comes from the upper 275-keV transition, and the γ-ray intensity ratio between the upper 275- and the 294-keV transitions should be the same as that in the singles spectrum. Thus, the γ-ray intensity of the upper 275-keV transition was obtained as the product of this ratio and the γ-ray intensity of the 294-keV transition in the singles spectrum, while the γ-ray intensity of the lower 275-keV transition was obtained by subtracting that of the upper 275-keV transition from the doublet 275-keV transition. Similarly, the γ-ray intensity of the lower 358-keV transition was obtained by comparing the intensities of the 316- and 358-keV peaks in the 294-keV coincident spectrum, while the intensity of the 316-keV transition was extracted in the singles spectrum. For the γ-ray intensities extracted in the coincident spectra, random coincidences were considered, and GEANT4 simulations were performed to correct coincidence efficiencies originating from angular correlation. The γ-ray intensities extracted in the present experiment and those from Ref. [22] are presented in Table I.

D. The lifetimes of the 6_1^- and 6_2^- states in ^{146}Eu

The lifetime of the 6_1^- state in ^{146}Eu was extracted through the coincidence between the 377- and 275-keV transitions. As shown in Fig. 7, the 358- and 377-keV γ rays cannot be separated by the $LaBr_3$(Ce) detector in the 275-keV gated spectrum. Bi-Gaussian plus linear functions were used to fit the gated spectrum near 370 keV, and the standard deviations of these two Gaussian functions are both about 13 keV. The influence of the 358-keV transition can be effectively reduced by choosing an appropriate energy gate based on the distributions of the 358- and 377-keV peaks. Thus we set one gate at 395 ± 5 keV (area S_2 in Fig. 7) and another gate at 275 ± 15 keV for γ-γ coincidence to analyze the lifetime of the 6_1^- state, where the 275-keV γ ray is taken as a decay transition. The delayed and antidelayed time-difference distributions are shown in Fig. 8(a). A similar background-timing correction procedure (see Sec III B) is applied, and the true time centroid difference for the 395-275 keV combination was found to be $\Delta C_{6_1^-}(395\text{-}275) = 58(5)$ ps. The lifetime of the 6_1^- state was determined as $\tau_{6_1^-} = 3^{+5}_{-3}$ ps, i.e., $\tau_{6_1^-} \leqslant 8$ ps.

The lifetime of the 6_2^- state was also extracted in the same way. Similarly, we set one gate at 275 ± 15 keV, and another gate at 340 ± 5 keV (area S_1 in Fig. 7) to avoid the influence of the 377 keV γ ray, where the 275-keV γ ray is considered as feeding transition. Figure 8(b) presents the delayed and antidelayed time distributions. After the background-timing correction, the true centroid difference is $\Delta C_{\text{total}}(275\text{-}340) = 19(5)$ ps. The subscript "total" denotes that this centroid difference contains the lifetime information of the 6_1^- and 6_2^- states. We derived the true centroid difference of the 6_2^- state for the 275-340 keV combination following

$$\Delta C_{6_2^-} = (1+\alpha)\Delta C_{\text{total}} - \alpha \Delta C_{6_1^-}, \tag{4}$$

where $\Delta C_{6_1^-}$ for the 275-340 keV combination was calculated as $\Delta C_{6_1^-} = -40(13)$ ps according to Eq. (2) using the PRD and lifetime of the 6_1^- state, while α is the γ coincidence intensity ratio between the $358 \rightarrow 275$ and $275 \rightarrow 358$ cascades.

TABLE I. Relevant γ transitions below the 9^+ isomer in ^{146}Eu. The BRICC code [34] was employed to obtain the internal conversion coefficient (ICC) from the mixing ratio (δ) or vice versa.

γ(keV)	$J_i^\pi \to J_f^\pi$ [24]	Multipolarity	$\lvert\delta\rvert$	ICC	γ-ray intensity Ref. [22]	γ-ray intensity Present work
14.5(1)[a]	$5_1^- \to 4^-$	$M1+E2$	<0.035[d]	74(26)[f]	3(1)	
56.2(1)[a]	$6_2^- \to 5_2^-$	$M1+E2$	<0.35[d]	9.7(13)[f]	0.23(3)	
83.2(2)[a]	$6_2^- \to 6_1^-$	$M1+E2$		4(1)[g]	⩽0.2	
275.0(2)[b]	$7^- \to 6_2^-$	$M1+E2$	<0.55[e]	0.109^{+4}_{-7}[h]	32(16)	62(8)[i]
275.0(2)[b]	$6_1^- \to 5_1^-$	$M1+E2$	<0.55[e]	0.109^{+4}_{-7}[h]	170(16)	147(20)[i]
293.5(2)[b]	$9^+ \to 6_2^-$	$E3$[c]		0.254(4)	3.9(2)	3.9(4)[j]
316.2(2)[b]	$5_2^- \to 4^-$	$M1+E2$	<0.6[e]	0.074^{+4}_{-6}[h]	2.3(2)	2.3(2)[j]
358.2(2)[b]	$7^- \to 6_1^-$	$M1+E2$	<0.5[e]	0.054^{+2}_{-4}[h]	75(18)	31(6)[i]
358.2(2)[b]	$6_2^- \to 5_1^-$	$M1+E2$	<0.5[e]	0.054^{+2}_{-4}[h]	36(18)	81(15)[i]
377.0(1)[b]	$9^+ \to 6_1^-$	$E3$[c]		0.099(2)	100	100[j]

[a]Energy reported in Ref. [22].
[b]Energy measured in the present work.
[c]Pure $E3$ transition according to the measured α_K value reported in Ref. [22].
[d]The upper limit of mixing ratio was estimated based on the total ICC.
[e]The upper limit of mixing ratio was estimated based on the experimental α_K value [22].
[f]Total ICC deduced from intensity balance.
[g]The average of $M1$ and $E2$ ICC values, and its uncertainty covers the pure $M1$ and $E2$ ICC values.
[h]The central value of ICC was obtained by taking the mixing ratio as half of its upper limit. Its upper (lower) uncertainty corresponds to the difference between ICC($\delta = 0$) [ICC(δ = upper limit)] and the central value.
[i]Intensity deduced from the γ-γ coincidence spectra.
[j]Intensity deduced from the singles spectrum.

The γ coincidence intensity of each cascade was obtained as the product of intensity of the feeding γ ray and the branching ratio of decay γ ray, where all decay routes, including γ decay and internal conversion, were considered (the adopted ICC values were listed in Table I). Using the γ-ray intensities extracted in the present work, α was deduced as $\alpha = 0.49(12)$. Then the true centroid difference of the 6_2^- state was obtained as $\Delta C_{6_2^-}(275\text{-}340) = 48(12)$ ps, and the lifetime of the 6_2^- state was extracted to be $\tau_{6_2^-} = 41(7)$ ps.

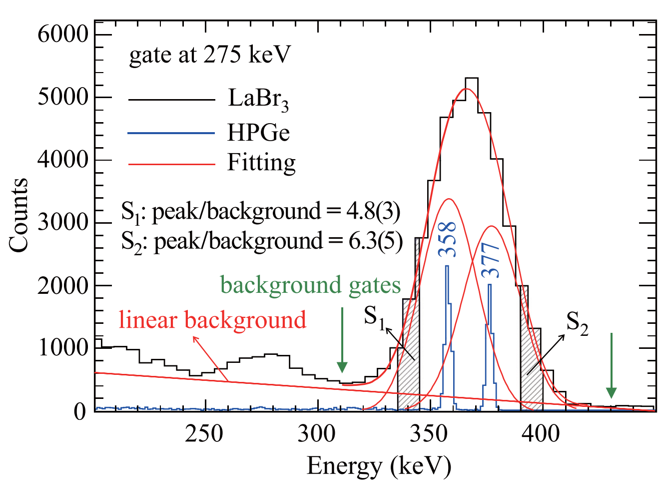

FIG. 7. Coincident γ-ray spectra gated on the 275-keV peak measured between 10 and 700 μs after the ERs were implanted in the SSD. The histogram in black is the LaBr$_3$(Ce) spectrum, and the histogram in blue is the HPGe spectrum, The red lines are the fitted curves. A linear background underneath the photopeak was considered.

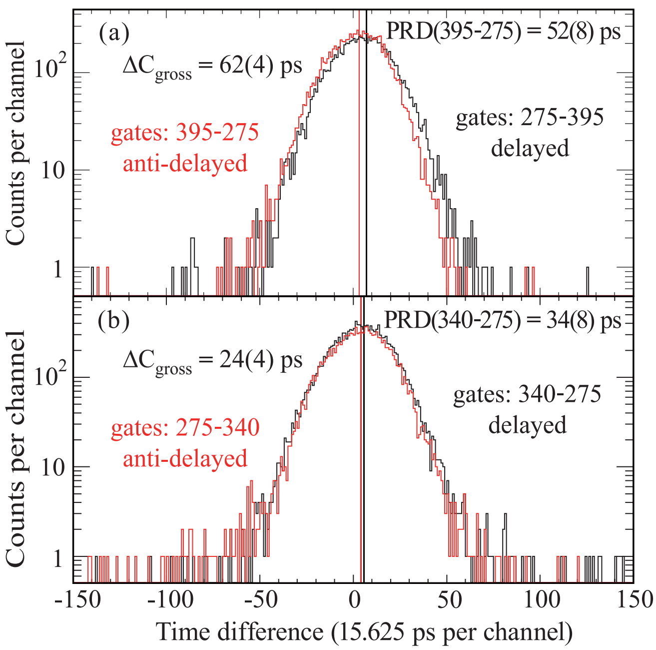

FIG. 8. Panel (a) presents the delayed and antidelayed time-difference spectra for the 6_1^- state in ^{146}Eu. Panel (b) shows the delayed and antidelayed time-difference spectra of the 340-275 keV combination, containing the lifetime information of the 6_1^- and the 6_2^- states in ^{146}Eu.

TABLE II. The results of the shell model calculations using KH5082, CWG, and CW5082 interactions are compared with the experimental data. The superscript *e* (*o*) indicates that the orbital is occupied by an even (odd) number of nucleons. The calculated levels were matched to the experimental one based on the reduced transition probabilities.

Expt.		KH5082		CWG		CW5082	
Energy (keV)	J^π	Energy (keV)	Configuration	Energy (keV)	Configuration	Energy (keV)	Configuration
Dominated by $\pi d_{5/2}^{-1}\nu f_{7/2}$							
0	4_1^-	0	$[\pi(g_{7/2}^e, d_{5/2}^o)\nu(f_{7/2}^1)]$ (80.59%)	0	$[\pi(g_{7/2}^e, d_{5/2}^o)\nu(f_{7/2}^1)]$ (61.65%)	0	$[\pi(g_{7/2}^e, d_{5/2}^o)\nu(f_{7/2}^1)]$ 68.05%)
			$+[\pi(g_{7/2}^o, d_{5/2}^e)\nu(f_{7/2}^1)]$ (8.10%)		$+[\pi(g_{7/2}^o, d_{5/2}^e)\nu(f_{7/2}^1)]$ (10.89%)		$+[\pi(g_{7/2}^o, d_{5/2}^e)\nu(f_{7/2}^1)]$ (7.27%)
14.4	5_1^-	59	$[\pi(g_{7/2}^e, d_{5/2}^o)\nu(f_{7/2}^1)]$ (72.61%)	16	$[\pi(g_{7/2}^e, d_{5/2}^o)\nu(f_{7/2}^1)]$ (56.08%)	31	$[\pi(g_{7/2}^e, d_{5/2}^o)\nu(f_{7/2}^1)]$ (72.84%)
			$+[\pi(g_{7/2}^o, d_{5/2}^e)\nu(f_{7/2}^1)]$ (10.19%)		$+[\pi(g_{7/2}^o, d_{5/2}^e)\nu(f_{7/2}^1)]$ (24.49%)		$+[\pi(g_{7/2}^o, d_{5/2}^e)\nu(f_{7/2}^1)]$ (9.54%)
289.3	6_1^-	404	$[\pi(g_{7/2}^e, d_{5/2}^o)\nu(f_{7/2}^1)]$ (89.55%)	230	$[\pi(g_{7/2}^e, d_{5/2}^o)\nu(f_{7/2}^1)]$ (80.06%)	208	$[\pi(g_{7/2}^e, d_{5/2}^o)\nu(f_{7/2}^1)]$ (51.92%)
			$+[\pi(g_{7/2}^o, d_{5/2}^e)\nu(f_{7/2}^1)]$ (2.49%)		$+[\pi(g_{7/2}^o, d_{5/2}^e)\nu(f_{7/2}^1)]$ (4.14%)		$+[\pi(g_{7/2}^o, d_{5/2}^e)\nu(f_{7/2}^1)]$ (33.64%)
Dominated by $\pi g_{7/2}^{-1}\nu f_{7/2}$							
316.6	5_2^-	130	$[\pi(g_{7/2}^o, d_{5/2}^e)\nu(f_{7/2}^1)]$ (77.54%)	60	$[\pi(g_{7/2}^o, d_{5/2}^e)\nu(f_{7/2}^1)]$ (51.56%)	138	$[\pi(g_{7/2}^o, d_{5/2}^e)\nu(f_{7/2}^1)]$ (65.23%)
			$+[\pi(g_{7/2}^e, d_{5/2}^o)\nu(f_{7/2}^1)]$ (7.87%)		$+[\pi(g_{7/2}^e, d_{5/2}^o)\nu(f_{7/2}^1)]$ (24.71%)		$+[\pi(g_{7/2}^e, d_{5/2}^o)\nu(f_{7/2}^1)]$ (10.2%)
372.6	6_2^-	136	$[\pi(g_{7/2}^o, d_{5/2}^e)\nu(f_{7/2}^1)]$ (86.63%)	98	$[\pi(g_{7/2}^o, d_{5/2}^e)\nu(f_{7/2}^1)]$ (76.34%)	151	$[\pi(g_{7/2}^o, d_{5/2}^e)\nu(f_{7/2}^1)]$ (45.93%)
			$+[\pi(g_{7/2}^e, d_{5/2}^o)\nu(f_{7/2}^1)]$ (2.31%)		$+[\pi(g_{7/2}^e, d_{5/2}^o)\nu(f_{7/2}^1)]$ (4.28%)		$+[\pi(g_{7/2}^e, d_{5/2}^o)\nu(f_{7/2}^1)]$ (35.60%)
647.5	7_1^-	511	$[\pi(g_{7/2}^o, d_{5/2}^e)\nu(f_{7/2}^1)]$ (86.84%)	475	$[\pi(g_{7/2}^o, d_{5/2}^e)\nu(f_{7/2}^1)]$ (78.46%)	423	$[\pi(g_{7/2}^o, d_{5/2}^e)\nu(f_{7/2}^1)]$ (77.48%)
			$+[\pi(g_{7/2}^e, d_{5/2}^o)\nu(f_{7/2}^1)]$ (2.19%)		$+[\pi(g_{7/2}^e, d_{5/2}^o)\nu(f_{7/2}^1)]$ (2.56%)		$+[\pi(g_{7/2}^e, d_{5/2}^o)\nu(f_{7/2}^1)]$ (1.18%)

IV. DISCUSSION

The previous studies of Refs. [22,24] have pointed out that the low-lying states below the 9^+ isomer in ^{146}Eu result from the coupling of the one proton hole to one neutron particle outside the ^{146}Gd core. Among these states, it is apparent that the 7^- and 9^+ states are the maximum aligned members of the $\pi g_{7/2}^{-1}\nu f_{7/2}$ and $\pi h_{11/2}\nu f_{7/2}$ multiplets, respectively. In the present measurements, the reduced transition probability of the $9^+ \rightarrow 6_1^-$ transition is five times larger than that of the $9^+ \rightarrow 6_2^-$ transition, in agreement with the previous work [24]. The main components of the 6_1^- and 6_2^- states were suggested to be $\pi d_{5/2}^{-1}\nu f_{7/2}$ and $\pi g_{7/2}^{-1}\nu f_{7/2}$, respectively, since that spin-flip transition is less favored than non-spin-flip one. It is worth noting that the priority of the $\pi h_{11/2} \rightarrow \pi d_{5/2}$ can be attributed by another mechanism, that is the possible enhanced $E3$ transition between two orbitals with $\Delta l = \Delta j = 3$. The $7^- \rightarrow 6_1^-$ transition is expected to be significantly hindered due to the l-forbidden mechanism [35], with a typical $B(M1)$ value of 10^{-2} – 10^{-3} W.u. in this mass region, while $B(M1)$ would be close to 1 W.u. for the $7^- \rightarrow 6_2^-$ transition connecting members of the same multiplet. Thus, one expects that the $B(M1)$ value of the latter transition is significantly larger than that of the former. However, the $B(M1)$ values for the two transitions were found to be almost equal in the previous experiment by Ercan *et al.* [22]. Unfortunately, the experimental proofs supporting the reported intensities were absent in Ref. [22], preventing further comparison. Based on the γ-ray intensities measured in the present work, the extracted $B(M1)$ values for the $7^- \rightarrow 6_2^-$ and $7^- \rightarrow 6_1^-$ transitions differ by a factor of 4.4, in agreement with the suggested configuration assignments. Additionally, the $B(M1)$ ratio between these two transitions should be about 10^2 if the configurations of these two 6^- states are pure. Thus, the small ratio of 4.4 indicates considerable configuration mixing.

As mentioned earlier, there is a discrepancy on the configuration assignment to the 5_1^- state in the previous works [21,22,24]. In the present work, the reduced $M1$ transition probabilities of the $6_1^- \rightarrow 5_1^-$ and $6_2^- \rightarrow 5_1^-$ transitions in ^{146}Eu are extracted to be $B(M1; 6_1^- \rightarrow 5_1^-) > 0.135$ W.u. and $B(M1; 6_2^- \rightarrow 5_1^-) = 0.015(4)$ W.u., respectively. The $B(M1)$ values indicate that the $6_2^- \rightarrow 5_1^-$ transition indeed has the nature of an l-forbidden $M1$ transition, and thus the dominant configuration of the 5_1^- level is $\pi d_{5/2}^{-1}\nu f_{7/2}$, in agreement with Refs. [22,24]. In addition, the energy of the 2_1^+ state in ^{146}Gd

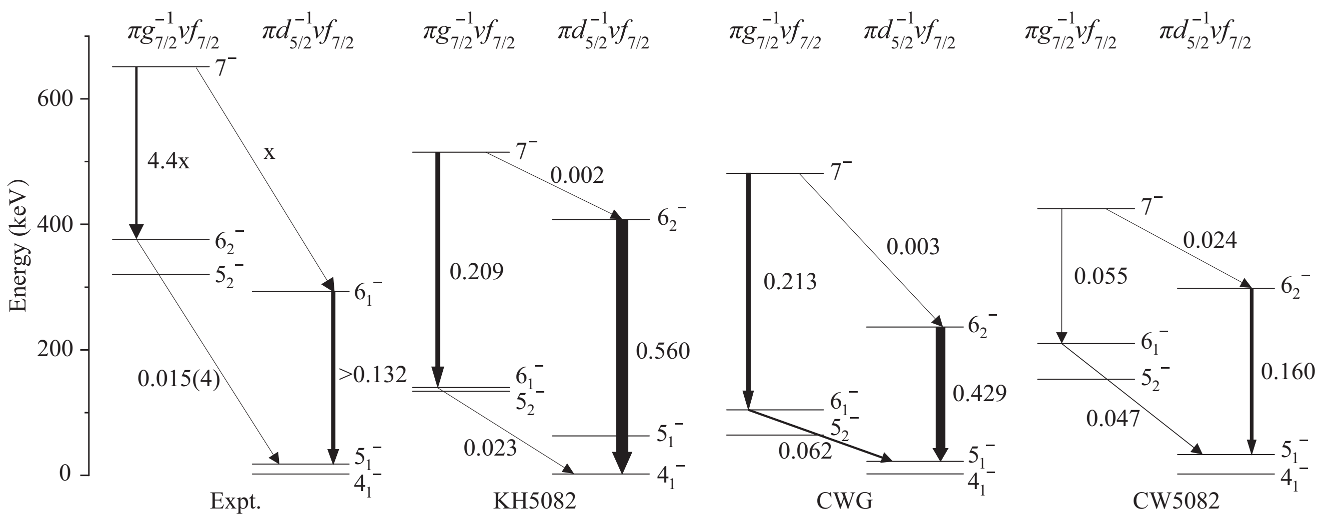

FIG. 9. The results of the shell model calculations using the KH5082, CWG, and CW5082 interactions, the experimental data was also presented. In each level scheme, the levels were divided on the left and right sides by the multiplet they belong to. The widths of the arrows are proportional to the reduced transition probabilities, which were marked near the arrow in Weisskopf units (W.u.).

is 1.97 MeV [12], suggesting that core excitation does not have a considerable contribution to the low-lying states. The 302-keV energy gap between the two 5^- states [24] indicates a relatively pure configuration for each of them. Thus, the main configuration component of 5_2^- level is expected to be $\pi g_{7/2}^{-1} \nu f_{7/2}$.

Large-scale shell model calculations were performed using the CWG [36], KH5082, and CW5082 [37] interactions, taking ^{132}Sn as the doubly closed core. The model space consists of the $\pi(1g_{7/2}, 2d_{5/2}, 2d_{3/2}, 3s_{1/2}, 1h_{11/2})$ and $\nu(2f_{7/2}, 1h_{9/2}, 2f_{5/2}, 3p_{3/2}, 3p_{1/2}, 1i_{13/2})$ single-particle orbitals. Table II lists the experimental and theoretical energies as well as the corresponding main configuration components of the low-lying states in ^{146}Eu. Figure 9 shows the reduced transition probabilities deduced from the present experiment in comparison with the corresponding shell model results. Due to the limited predictive power of the shell model in excitation energies, especially for odd-odd nuclei, the ordering of levels given by the shell model calculations is not necessarily consistent with that of experiment. In fact, it is the reduced transition probability that can probe the nuclear structure of the initial and final states, and we matched the calculated level to the experimental one by comparing the reduced transition probabilities. As listed in Table II, the main configuration components given by all employed effective interactions are in agreement with the present experimental expectations.

In the shell model calculations, a nonzero $B(M1)$ value between the $\pi g_{7/2}^{-1} \nu f_{7/2}$ and $\pi d_{5/2}^{-1} \nu f_{7/2}$ multiplets is understood to result from configuration mixing, and the amplitude of configuration mixing is inversely proportional to the energy gap. The ratio between $B(M1; 7^- \rightarrow 6_2^-)$ and $B(M1; 7^- \rightarrow 6_1^-)$ is extracted based on the experimental γ-ray intensities. In the present theoretical results, this ratio mainly depends on the amplitude of configuration mixing between the two 6^- levels, because all interactions give a relatively pure configuration component for the 7^- state. The CWG and KH5082 interactions give a much larger $B(M1)$ ratio between these two transitions, which reflects an underestimation of configuration mixing between the two 6^- states. The CW5082 interaction gives a $B(M1)$ ratio of about 2.2, which reflects the considerable mixing of the $\pi d_{5/2}^{-1} \nu f_{7/2}$ and $\pi g_{7/2}^{-1} \nu f_{7/2}$ configurations, and reproduces the experimental result best. The experimental $B(M1)$ ratio between the $6_2^- \rightarrow 5_1^-$ and $6_1^- \rightarrow 5_1^-$ transitions was also calculated. This $B(M1)$ ratio given by the three interactions was found to be of the same order of magnitude as the experimental one, while CWG and CW5082 give relatively large ratios.

In the ^{142}Pr, ^{144}Pm, and ^{146}Eu isotones, similar decay patterns were observed for the 7^-, 6^-, and 5^- states. These states in ^{142}Pr and ^{144}Pm are interpreted in terms of configuration mixing of the $\pi d_{5/2}^{-1} \nu f_{7/2}$ and $\pi g_{7/2}^{-1} \nu f_{7/2}$ multiplets [40–42], but the main configuration components were not clear. Based on the similarity of the level structure as well as the $B(M1)$ ratio between the $7^- \rightarrow 6_2^-$ and $7^- \rightarrow 6_1^-$ transitions, the dominant configurations can be assigned respectively to the low-lying states in ^{142}Pr and ^{144}Pm, as shown in Fig. 10. In the three isotones, the energies of the 7^- levels and the energy differences between two 6^- states increase with proton number, which can be attributed to the increase of the energy gap between the $2d_{5/2}$ and $1g_{7/2}$ proton orbitals. For ^{146}Eu, the largest $B(M1)$ ratio between the $7^- \rightarrow 6_2^-$ and $7^- \rightarrow 6_1^-$ transitions is observed due to the largest energy differences between the two 6^- states. A common feature for these three isotones is that the energies of the 5^- and 6^- states belonging to the $\pi g_{7/2}^{-1} \nu f_{7/2}$ multiplet are higher than those of the 5^- and 6^- states belonging to the $\pi d_{5/2}^{-1} \nu f_{7/2}$ multiplet. However, it is not reproduced by the shell model calculations performed for ^{146}Eu in the present work. This discrepancy might be due to the complicated two-body interaction between the 13 protons with respect to the ^{132}Sn core in the shell model calculation. Better descriptions of nuclei in the vicinity of ^{146}Gd would be achieved by taking ^{146}Gd as the core and allowing certain

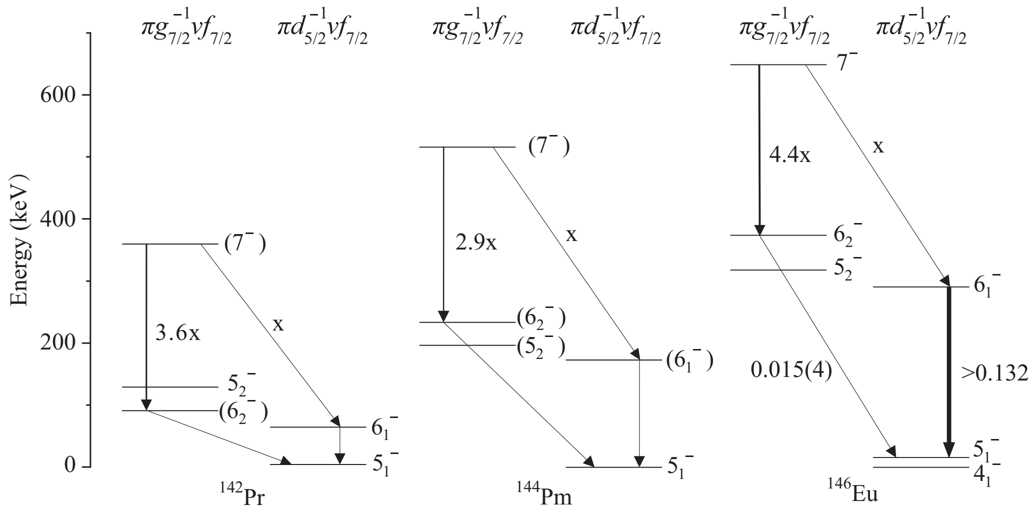

FIG. 10. The systematics of level structure in ^{142}Pr, ^{144}Pm, and ^{146}Eu. The known reduced transition probabilities in W.u. were marked near the arrows. The $B(M1)$ ratios in ^{142}Pr and ^{144}Pm were calculated based on the relevant γ-ray intensities reported in Refs. [38,39], respectively, assuming pure $M1$ character for simplicity.

core excitations, in case all the necessary nucleon-nucleon interactions are extracted from the nuclei close to ^{146}Gd.

V. SUMMARY

In the present work, the lifetimes of the 6_1^- and 6_2^- levels were measured employing the MSCD method with fast-timing LaBr$_3$(Ce) detectors, and the γ-ray intensities of the 275- and 358-keV doublet transitions were re-analyzed using HPGe detectors. The $B(M1)$ values of the $6_1^- \rightarrow 5_1^-$ and $6_2^- \rightarrow 5_1^-$ transitions were deduced, and the configurations of the 6^- and 5^- levels are proposed by comparing the experimental results with the shell model calculations. In particular, our results clearly show that the 5_1^- state has a dominant $\pi d^{-1}_{5/2} \nu f_{7/2}$ configuration, solving the discrepancy in its configuration assignment proposed in previous works.

ACKNOWLEDGMENTS

We are grateful to the accelerator staff of HIRFL for providing a stable ^{27}Al beam. This work was supported by the National Natural Science Foundation of China (Grants No. 12135004, No. 11961141004, No. 11635003, No. U2032135, No. U1932137, No. 11805243, and No. 11975282), the Strategic Priority Research Program of the Chinese Academy of Sciences (Grant No. XDB34000000), the National Key R&D Program of China (Contract No. 2018YFA0404402), the Key Research Program of the Chinese Academy of Sciences (Grant No. XDPB15), and Guangdong Major Project of Basic and Applied Basic Research (Grant No. 2021B0301030006). The theoretical calculations were performed using the computing resources of Gansu Advanced Computing Center.

[1] L. Coraggio, A. Covello, A. Gargano, N. Itaco, and T. T. S. Kuo, Realistic shell-model calculations for proton particle-neutron hole nuclei around ^{132}Sn, Phys. Rev. C **66**, 064311 (2002).

[2] J. P. Schiffer and W. W. True, The effective interaction between nucleons deduced from nuclear spectra, Rev. Mod. Phys. **48**, 191 (1976).

[3] O. Sorlin and M. G. Porquet, Nuclear magic numbers: New features far from stability, Prog. Part. Nucl. Phys. **61**, 602 (2008).

[4] P.-A. Söderström *et al.*, Two-hole structure outside ^{78}Ni: Existence of a μs isomer of ^{76}Co and β decay into ^{76}Ni, Phys. Rev. C **92**, 051305(R) (2015).

[5] A. Jungclaus *et al.*, First observation of γ rays emitted from excited states south-east of ^{132}Sn: The $\pi g^{-1}_{9/2} \otimes \nu f_{7/2}$ multiplet of ^{132}In$_{83}$, Phys. Rev. C **93**, 041301 (2016).

[6] V. H. Phong *et al.*, Observation of a μs isomer in $^{134}_{49}$In$_{85}$: Proton-neutron coupling "southeast" of $^{132}_{50}$Sn$_{82}$, Phys. Rev. C **100**, 011302 (2019).

[7] C. Cline, W. Alford, H. Gove, and R. Tickle, Multiplet structure of ^{210}Bi from the ^{209}Bi(d,p) and ^{209}Bi(α, ^{3}He) reactions, Nucl. Phys. A **186**, 273 (1972).

[8] W. P. Alford, J. P. Schiffer, and J. J. Schwartz, Proton-Particle, Neutron-Hole Multiplets in Bi-208, Phys. Rev. Lett. **21**, 156 (1968).

[9] C. Ellegaard, P. D. Barnes, R. Eisenstein, and T. R. Canada, Decay modes and lifetimes of the levels in the $\pi h_{9/2} \nu g_{9/2}$ multiplet in ^{210}Bi, Phys. Lett. B **35**, 145 (1971).

[10] R. Tickle and J. Bardwick, Two-proton multiplets in ^{210}Po, Phys. Lett. B **36**, 32 (1971).

[11] A. Molinari, W. M. Alberico, M. B. Johnson, and H. A. Bethe, Effective two body interaction in simple nuclear spectra, Nucl. Phys. A **239**, 45 (1975).

[12] M. Ogawa, R. Broda, K. Zell, P. J. Daly, and P. Kleinheinz, Lowest 2^+ State in $^{146}_{64}$Gd$_{82}$ and the Energy Gap at $Z = 64$, Phys. Rev. Lett. **41**, 289 (1978).

[13] R. F. Casten, D. D. Warner, D. S. Brenner, and R. L. Gill, Relation between the $Z = 64$ Shell Closure and the Onset

of Deformation at $N = 88$-90, Phys. Rev. Lett. **47**, 1433 (1981).

[14] R. R. Chasman, ^{147}Tb and proton single particle states near $Z = 64$, Phys. Rev. C **21**, 456 (1980).

[15] P. Kleinheinz, R. Broda, P. J. Daly, S. Lunardi, M. Ogawa, and J. Blomqvist, Particle hole yrast states in ^{146}Gd and ^{147}Gd and the Z = 64 shell closure, Z. Phys. A **290**, 279 (1979).

[16] A. Bohr and B. R. Mottelson, *Nuclear Structure Vol. 1: Single-Particle Motion* (World Scientific, 1999)

[17] R. F. Casten, *Nuclear Structure from a Simple Perspective* (Oxford University Press, Oxford, 2001).

[18] S. W. Yates, E. E. Peters, A. Chakraborty, B. P. Crider, M. T. McEllistrem, F. M. Prados-Estévez, and J. R. Vanhoy, Level lifetimes in ^{94}Zr from DSAM measurements following inelastic neutron scattering, EPJ Web Conf. **66**, 02111 (2014).

[19] A. Dewald, O. Moller, and P. Petkov, Developing the Recoil Distance Doppler-Shift technique towards a versatile tool for lifetime measurements of excited nuclear states, Prog. Part. Nucl. Phys. **67**, 786 (2012).

[20] P. Walker and Z. Podolyák, 100 years of nuclear isomers—then and now, Phys. Scr. **95**, 044004 (2020).

[21] T. Bhattacharjee, D. Banerjee, S. K. Das, S. Chanda, T. Malik, A. Chowdhury, P. Das, S. Bhattacharyya, and R. Guin, Spectroscopy of low-lying states in odd-odd ^{146}Eu, Phys. Rev. C **88**, 014313 (2013).

[22] A. Ercan, R. Broda, P. Kleinheinz, M. Piiparinen, R. Julin, and J. Blomqvist, The two particle-phonon multiplet $\pi h_{11/2} \nu f_{7/2} \times 3^-$ and higher-lying four-nucleon yrast states in the doubly-odd nucleus $^{146}_{63}$Eu$_{83}$, Z. Physik A - Atomic Nuclei **329**, 63 (1988).

[23] A. Islam, A. G. Lee, and R. G. Summers-Gill, The Particle-Hole Nucleus ^{146}Eu, Technical Report, McMaster University, 1981 (unpublished).

[24] A. Ercan, R. Broda, M. Piiparinen, Y. Nagai, R. Pengo, and P. Kleinheinz, The 235 μs 9^+ isomer in ^{146}Eu, Z. Phys. A **295**, 197 (1980).

[25] R. Kantus, U. J. Schrewe, W. D. Schmidt-Ott, and R. Michaelsen, Decay properties of ^{146}Gd, Phys. Rev. C **23**, 1274 (1981).

[26] G. Borchert, J. Bojowald, A. Ercan, H. Labus, T. Rose, and O. Schult, Curved crystal spectrometer for high-resolution in-beam spectroscopy of x-rays and low-energy gamma rays, Nucl. Instrum. Methods Phys. Res., Sect. A **245**, 393 (1986).

[27] Z. Zhang, L. Ma, Z. Gan, M. Huang, T. Huang, G. Li, X. Wu, G. Jia, L. Yu, H. Yang, Z. Sun, X. Zhou, H. Xu, and W. Zhan, A gas-filled recoil separator, SHANS, Nucl. Instrum. Methods Phys. Res., Sect. B **317**, 315 (2013).

[28] J.-M. Régis, G. Pascovici, J. Jolie, and M. Rudigier, The mirror symmetric centroid difference method for picosecond lifetime measurements via γ-γ coincidences using very fast LaBr$_3$(Ce) scintillator detectors, Nucl. Instrum. Methods Phys. Res., Sect. A **622**, 83 (2010).

[29] J.-M. Régis, Fast timing with LaBr$_3$(Ce) scintillators and the mirror symmetric centroid difference method, Ph.D. thesis, University of Cologne, 2011.

[30] J. M. Régis *et al.*, The Generalized Centroid Difference method for lifetime measurements via γ-γ coincidences using large fast-timing arrays, EPJ Web Conf. **93**, 01013 (2015).

[31] J. Adam, J. Dobeš, B. Kracík, P. Navrátil, P. Tlustý, S. Batsev, T. K. Dinh, M. Grinberg, O. Stoyanova, and Ch. Stoyanov, Structure of the ^{146}Sm states from the ^{146}Eu decay, Z. Physik A - Hadrons and Nuclei **343**, 381 (1992).

[32] S. Rozak, E. G. Funk, and J. W. Mihelich, Recoil distance lifetime measurements in ^{146}Sm, Phys. Rev. C **25**, 3000 (1982).

[33] Y. Khazov, A. Rodionov, and G. Shulyak, Nuclear data sheets for A = 146, Nucl. Data Sheets **136**, 163 (2016).

[34] https://bricc.anu.edu.au/.

[35] W. Andrejtscheff, L. Zamick, N. Z. Marupov, K. M. Muminov, and T. M. Muminov, Core polarization for l-forbidden M1 transitions in light nuclei, Nucl. Phys. A **351**, 54 (1981).

[36] B. A. Brown, N. J. Stone, J. R. Stone, I. S. Towner, and M. Hjorth-Jensen, Magnetic moments of the 2_1^+ states around ^{132}Sn, Phys. Rev. C **71**, 044317 (2005).

[37] S. Sarkar and M. S. Sarkar, Shell model study of neutron rich nuclei near ^{132}Sn, Phys. Rev. C **64**, 014312 (2001).

[38] C. Bercks, E. Hummel, and K. H. Schedl, Untersuchung der Struktur des *u-u*-Kerns ^{142}Pr durch (α, nγ)- und (p, nγ)-Reaktionen und Bestimmung von Matrixelementen der effektiven Proton-Neutron-Restwechselwirkung, Z. Phys. A **273**, 385 (1975).

[39] https://www.nndc.bnl.gov/ensdf/.

[40] J. Kern, G. L. Struble, R. K. Sheline, E. T. Jurney, H. R. Koch, B. P. K. Maier, U. Gruber, and O. W. B. Schult, Nuclear levels in ^{142}Pr, Phys. Rev. **173**, 1133 (1968).

[41] M. Macphail and R. Summers-gill, The doubly odd nucleus ^{144}Pm (I). Energy levels, Nucl. Phys. A **237**, 285 (1975).

[42] M. Macphail and R. Summers-Gill, The doubly odd nucleus ^{144}Pm: (II). Interpretation, Nucl. Phys. A **263**, 12 (1976).